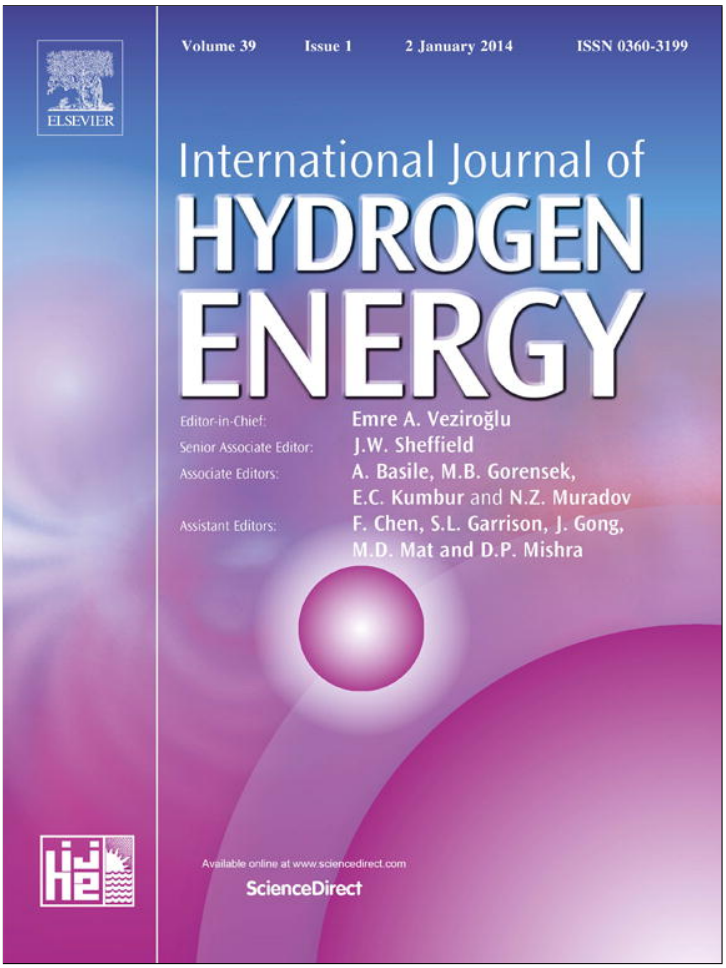

INTERNATIONAL JOURNAL OF HYDROGEN ENERGY 39 (2014) 231–248

Available online at www.sciencedirect.com

ScienceDirect

journal homepage: www.elsevier.com/locate/he

Fault-tolerant control design for safe production of hydrogen from bio-ethanol

P.A. Luppi [a,b], L. Nieto Degliuomini [a], M.P. García [a], M.S. Basualdo [a,c,*]

[a] Computer Aided Process Engineering Group (CAPEG), French Argentine International Center for Information and Systems Sciences (CIFASIS – CONICET – UNR – AMU), 27 de Febrero 210 bis, S2000EZP Rosario, Argentina
[b] FCEIA, Universidad Nacional de Rosario, Pellegrini 250, S2000EZP Rosario, Argentina
[c] Universidad Tecnologica Nacional – FRRo, Zeballos 1341, S2000BQA Rosario, Argentina

ARTICLE INFO

Article history:
Received 5 August 2013
Received in revised form
8 October 2013
Accepted 14 October 2013
Available online 16 November 2013

Keywords:
Fault-tolerant control system
Reconfigurable controller
Systematic methodology
Bio-ethanol processor
Fuel cell

ABSTRACT

This work presents a novel framework for fault-tolerant control design to achieve a safe and reliable production of hydrogen from bio-ethanol, which includes: (i) a nominal controller (NC) for fault-free operation, (ii) a reconfigurable controller (RC) for accommodate the faults anticipated at the design stage. The methodology produces alternative NC and RC solutions allowing to achieve a trade-off between performance and dimension of the structures, subject to the availability of healthy components. It is based on the evaluation of individual steady-state squared deviations in the context of Internal Model Control theory, and efficiently solved with genetic algorithms. The obtained structures are decentralized and can be implemented with conventional controllers. A reconfiguration mechanism which smoothly commissions the RC is also presented. The approach is tested in a hydrogen production plant to demonstrate its effectiveness against critical faults such as actuator blockade and loss of sensor measurement.

1. Introduction

Malfunctions in actuators, sensors or other system components can arise frequently during normal operation of industrial processes. As it is well-known, conventional control structures are not capable of implementing corrective actions for neutralize the effects of such faults. This could affect the process objectives due to unacceptable closed-loop performance or instability. Over the last decades, significant research in fault detection and diagnosis (FDD) [1,2], and alternative approaches in control design known as fault-tolerant control (FTC) [3–6] have been developed. The main motivations for introducing fault tolerance in a control system are [4]: (i) to increase the safety of the process, and (ii) to increase the reliability, i.e. the capacity of the system to properly implement the required actions over a certain period of time. In particular, any effort focused on the subject of safety involving production, manipulation and use of hydrogen is a main concern because it is a dangerous substance. Its lower flammability limit has a low value (4% by volume for hydrogen in air) which increases the combustion hazard [7].

* *Corresponding author*. Computer Aided Process Engineering Group (CAPEG), French Argentine International Center for Information and Systems Sciences (CIFASIS – CONICET – UNR – AMU), 27 de Febrero 210 bis, S2000EZP Rosario, Argentina. Tel.: +54 3414825106.
E-mail addresses: luppi@cifasis-conicet.gov.ar (P.A. Luppi), nieto@cifasis-conicet.gov.ar (L. Nieto Degliuomini), mgarcia@cifasis-conicet.gov.ar (M.P. García), basualdo@cifasis-conicet.gov.ar (M.S. Basualdo).
0360-3199/$ – see front matter
http://dx.doi.org/10.1016/j.ijhydene.2013.10.081

The existing reconfigurable FTC design strategies can be classified according to the utilized approach: multiple-model [8,9], H_∞ robust control [10,11], model predictive control [12,13], linear matrix inequality [14,15], sliding mode control [16,17] among others, and hybrid approaches [18–20]. Further investigation on novel design techniques with a good degree of systematics which can fit well in industrial applications remains an important issue [4,5]. Assuming that a FDD system is available for detecting and identifying a fault in time, this work presents a novel methodology for FTC design which satisfies the following requisites [21]: (i) *NC* structure reconfiguration subject to an efficient management of the remaining healthy components (redundancies) such that stability and acceptable closed-loop performance can be maintained, and (ii) *RC* implementation through a reconfiguration mechanism (RM) which tries to minimize the switching transients.

The proposed approach produces a set of alternative designs for *NC* and *RC* by employing a minimum number of controlled (CVs) and manipulated variables (MVs). This strategy is based on the novel procedure for decentralized control presented in Ref. [22] and the extended minimum squared deviations methodology proposed in Refs. [23,24]. Generating a reduced *NC* structure for normal operation allows redundancies availability. These additional resources has a strongly impact on the number of fault scenarios that the FTC system can deal with, as emphasized in Refs. [21,4]. In this study, typical faults such as valve sticking and complete loss of sensor measurement are considered. On the other hand, the methodology selects the optimal CVs and MVs for each structure by quantifying the *individual* steady-state squared deviations corresponding to the uncontrolled variables (UVs) and the MVs. This is done by assuming perfect control for the adopted CVs. This individual deviations analysis introduces several advantages: (i) to perform a trade-off between achievable performance and available hardware when a fault is considered, as suggested in Ref. [8], and (ii) to minimize the computational load at the dynamic simulation stage, because many candidate structures can be discarded directly at the design step. In fact, the individual steady-state deviations of the inputs/outputs can be used to predict unwanted dynamic behaviors. This represents a contribution to the work of [23,24] in the context of FTC design. Apart from this, the methodology solves the CVs–MVs selection simultaneously with the corresponding pairing task. Any of the algorithms discussed in Ref. [22] can be used to systematically obtain the best CVs–MVs pairing. This allows to apply the criterion proposed in Ref. [25] so as to check the stability of the obtained structures. This can be done in the three periods of system operations (fault-free period, transient period, and after the reconfiguration) as suggested in Ref. [4]. Finally, genetic algorithms (GA) propose an effective treatment for the above problems, with the advantage that it allows to evaluate several designed control structures, which can be sorted from the optimal one to the following suboptimal solutions [22,26]. Also, the risk of being trapped in local optima is minimal [27].

The proposed FTC system is restructurable [6] since the controller structure could be changed for most fault scenarios. For this purpose, a RM which minimizes the undesirable transients that might occur during the controller reconfiguration is implemented. It is worth noting that the transition management for reconfigurable control systems is still an open issue [10,28].

The approach is completely evaluated in the bio-ethanol fuel processor system (BPS) with fuel cell (FC) presented in Ref. [29]. This process involves bio-ethanol steam reforming, high and low temperature water gas shift reactors, and preferential oxidation. It is connected to a proton exchange membrane (PEM) FC for automotive purposes. Although the potentiality of the approach is demonstrated through this specific application, the methodology is intended to be: (i) systematic, because it tries to minimize the use of heuristic considerations, and (ii) generalized, because it can be applied independently of the case study. Even though the methodology does not depend on the dimension of the process, it is strongly based on the availability (and the effectiveness) of the redundancies. Once the (reduced) nominal control structure is obtained, what ensures this approach is the optimal utilization of the additional degrees of freedom to implement the FTC system. Anyway, a deeper analysis about the redundancies selection problem is under study.

Here, the performance of the FTC structure is analyzed through closed-loop simulations of the rigorous nonlinear process subject to the commented common faults in actuators/sensors, when the RM is activated/deactivated. The standard Urban Dynamometer Driving Schedule (UDDS) [30] is considered as load demand, which represents a typical and exigent disturbance for the system. Representative indexes are used for the sake of comparison and to support the final conclusions.

The work is organized as follows: the next section details the methodology for FTC design. It includes the design objectives, the proposed system architecture and fault scenarios, as well as the background of the design approach. This section also presents the developed RM, and the utilized tools to evaluate the potentiality of the approach. Section 3 starts with a brief description of the BPS with FC process and its objectives, and continues with the application of the methodology in order to design the FTC system. The simulation results, and also a detailed analysis of the dynamic behavior are presented in Section 4. Finally, in Section 5 the conclusions and future works are exposed.

2. Reconfigurable FTC design methodology

2.1. Objectives

In this study, the normal operating conditions as well as the potential faults are stated at the beginning, and the FTC system is designed to operate in all these modes.

For the fault-free mode, the objective is to design a square control configuration which uses a minimum number of CVs and MVs such that all process requirements are satisfied. This ensures that:

- the number of system components that can fail during normal operation is minimum, and

- there is availability of additional healthy control components, i.e. redundancies, for the RC design.

Once a specific fault is detected and isolated via a FDD scheme, the performance must be improved and the stability of the process must be guaranteed by switching from the NC to the appropriate RC_i.

This work extends the five-step procedure presented in Ref. [22] to be able to design the FTC system. It constitutes the principal contribution, which is detailed in Section 2.4. The overall tasks are schematically given in Fig. 1, involving:

1. Define the stabilizing control loops.
2. Obtain a simplified process model.
3. Find a minimum square configuration to satisfy the process requirements. Additional system resources remains available for managing specific faults.
4. Find an optimal decentralized structure to achieve acceptable performance degradation in the event of each fault.
5. Determine the tuning parameters of the selected control loops.
6. Evaluate the dynamic performance of the FTC system.

2.2. System architecture

Fig. 2 shows the architecture of the proposed FTC system. It consists of: a FDD scheme and decision mechanism, a nominal controller (NC), a reconfiguration mechanism and a reconfigurable controller (a set of RC_i). In the present work, a perfect FDD subsystem is assumed. Thus, the identification of a fault is simulated by a certain time delay. Here, the proposal is focused on the design of the NC and the RC_i, which is addressed in the framework of the Internal Model Control (IMC) theory.

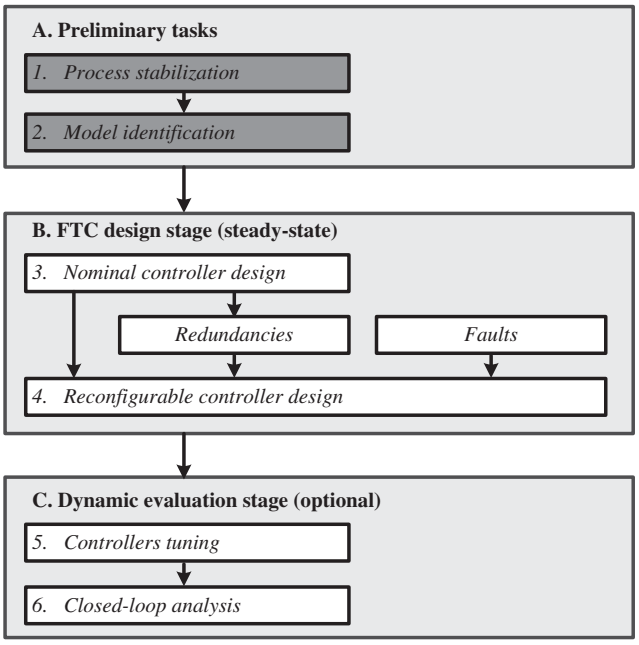

Fig. 1 – FTC design methodology.

2.3. Fault scenarios

In this paper, typical malfunctions in actuators and sensors are considered:

1. Actuator fault: it corresponds to a stuck valve, where the actuator no longer reacts to any control command. Thus, the number of MVs is reduced and the common controller actions for normal operation can not be implemented. In this context, the FTC design should be focused on minimize the performance degradation subject to the available MVs.
2. Sensor fault: it corresponds to the abrupt loss of a measurement. It is assumed that the correct information is not available, neither from physically redundant sensors nor from analytical redundancy. For this case, the objective is to minimize the deviation of the respective output from its operating point by the proper MVs management, keeping the overall performance.

2.4. FTC design approach

A graphical representation of the FTC operation philosophy is given in Fig. 3 where both the normal and fault cases are considered. The objective is to find an optimal decentralized structure within each feasible set which minimizes a pre-set performance criteria, subject to particular constraints. Therefore, the FTC system can compensate the effects of the different faults by switching from the NC to the appropriate RC_i through the reconfiguration actions.

The methodology proposed here involves the selection of q CVs from a set of m available outputs, and q MVs from a set of n available inputs, simultaneously with the $q \times q$ CVs–MVs pairing. Taking into account the well-known IMC structure presented in Fig. 4, at steady state ($s = 0$) the selected MVs ($\mathbf{u}_s$) and the UVs ($\mathbf{y}_r$) can be stated as [24,23]:

$$\mathbf{u}_s = \mathbf{G}_s^{-1}\mathbf{y}_s^{set} - \mathbf{G}_s^{-1}\mathbf{D}_s\mathbf{d} - \mathbf{G}_s^{-1}\mathbf{G}_s'\mathbf{G}_r \tag{1}$$

$$\mathbf{y}_r = \mathbf{G}_r\mathbf{G}_s^{-1}\mathbf{y}_s^{set} + (\mathbf{D}_r - \mathbf{G}_r\mathbf{G}_s^{-1}\mathbf{D}_s)\mathbf{d} + (\mathbf{D}_r' - \mathbf{G}_r\mathbf{G}_s^{-1}\mathbf{D}_s')\mathbf{u}_r \tag{2}$$

Here, $\mathbf{G}_s, \mathbf{D}_s, \mathbf{G}_s', \mathbf{G}_r, \mathbf{D}_r$, and $\mathbf{G}_r'$ are transfer function matrices of $q \times q, q \times p, q \times (n-q), (m-q) \times q, (m-q) \times p$, and $(m-q) \times (n-q)$, respectively. The vectors $\mathbf{y}_s^{set}$ and $\mathbf{d}$ of dimension $n \times 1$ and $p \times 1$ are setpoint and disturbance vectors, respectively.

As can be seen from Eq. (2), the deviation of the UVs respect to its nominal operating point due to set point modifications and disturbances depends specifically on the CVs–MVs selection through $\mathbf{G}_s$, $\mathbf{G}_r$, $\mathbf{D}_s$ and $\mathbf{D}_r$. Thus, the individual squared deviations of the UVs are available as the components of the following vector:

$$\mathbf{e}_{yr} = \sum_{i=1}^{n} \mathbf{e}_{yr_{set}}^2(i) + \sum_{j=1}^{p} \mathbf{e}_{yr_d}^2(j) \tag{3}$$

where

$$\mathbf{e}_{yr_{set}}(i) = (\mathbf{G}_r\mathbf{G}_s^{-1})\mathbf{y}_{set}^n(i) \tag{4}$$

$$\mathbf{e}_{yr_d}(j) = (\mathbf{D}_r - \mathbf{G}_r\mathbf{G}_s^{-1}\mathbf{D}_s)\mathbf{d}^p(j) \tag{5}$$

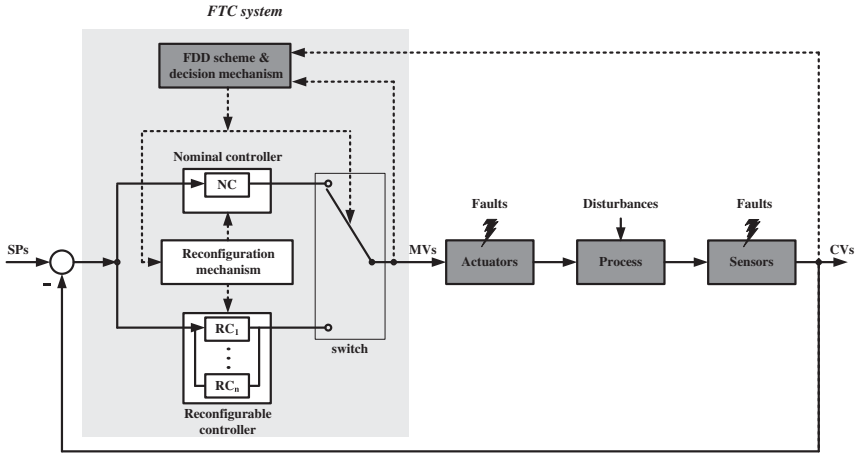

Fig. 2 – System architecture.

The vectors $\mathbf{y}^{n}_{set}(i)$ (dimension $n \times 1$) and $\mathbf{d}^{p}(j)$ (dimension $p \times 1$) have a unitary entry in the positions i and j respectively, and zero elsewhere. In addition, the individual squared deviations of the $\mathbf{u}_s(s)$ respect to their operating points are present in:

$$\mathbf{e}_{us} = \sum_{i=1}^{n} \mathbf{e}^2_{us_{set}}(i) + \sum_{j=1}^{p} \mathbf{e}^2_{us_d}(j) \tag{6}$$

where

$$\mathbf{e}_{us_{set}}(i) = (\mathbf{G}_s^{-1})\mathbf{y}^{n}_{set}(i) \tag{7}$$

$$\mathbf{e}_{us_d}(j) = (\mathbf{G}_s^{-1}\mathbf{D}_s)\mathbf{d}^{p}(j) \tag{8}$$

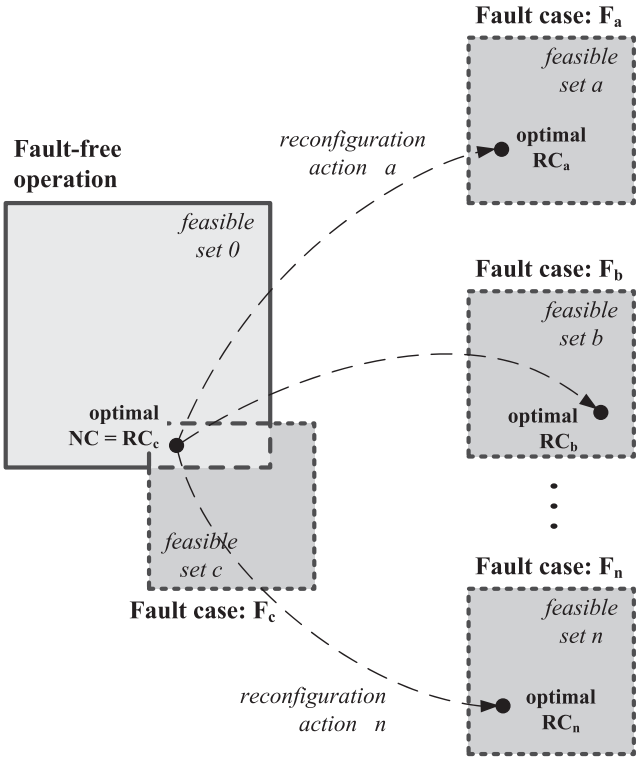

Fig. 3 – FTC operation philosophy.

The steady-state deviations of the UVs and the MVs given in Eqs. (3) and (6) allow to evaluate and compare different CVs–MVs combinations. This is useful for predicting (at the design stage) unwanted dynamic responses, as will be shown in Sections 3.3 and 4.

Generally, the determination of CVs–MVs sets based on the above procedure requires to do a great number of combinations for a selected q. GA is a stochastic global optimization method that mimics the metaphor of natural biological evolution, and produces a population of optimization solutions. Even though GA does not guarantee a global minimum, a great number of applications exist for solving problems of large dimension [22,27,26]. The advantage is that it produces a sorted set with the best solutions, which allows to evaluate them. In the framework of GA, the following binary chromosome (of dimension $m + n$) is proposed:

$$\mathbf{C}_i = [\mathbf{c}_i^{cv}, \mathbf{c}_i^{mv}] \tag{9}$$

where:

$$\mathbf{C}_i^{cv}(k) = [c_i^{cv}(1), \ldots, c_i^{cv}(m)] \tag{10}$$

$$\mathbf{C}_i^{mv}(j) = [c_i^{mv}(1), \ldots, c_i^{mv}(n)] \tag{11}$$

The genes in $\mathbf{C}_i^{cv}$ and $\mathbf{C}_i^{mv}$ represent the decision variables for the CVs and MVs selection, respectively. Here, $\mathbf{C}_i^{cv}(k) = 1$ indicates that the output corresponding to the location k is controlled, and the same applies to the inputs selection.

During normal operation, it is considered that no faults are present and the objective is to find a control configuration with a minimum number of control loops (a nominal controller, NC) focused on the quality of the plant behavior. Given a process with $m > n$, then for a selected q the proposed design procedure is to find a solution to minimize the performance criterion in Eq. (12) subject to the constraints of Eqs. (13)–(18):

$$\min_{(\mathbf{c}_i^{cv}, \mathbf{c}_i^{mv})} \left\| \mathbf{e}_{yr}(\mathbf{C}_i^{cv}, \mathbf{C}_i^{mv}) \right\|_1 \tag{12}$$

subject to:

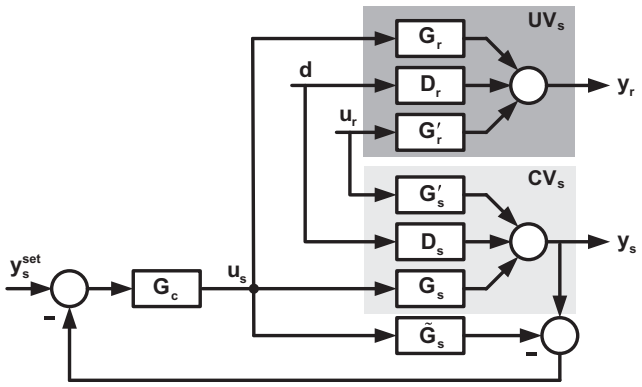

Fig. 4 – IMC structure.

$$\left\|\mathbf{C}_i^{mv}\right\|_1 = q \tag{13}$$

$$\left\|\mathbf{C}_i^{cv}\right\|_1 = q \tag{14}$$

$$\mathbf{e}_{yr}(\ell) \le \alpha, \quad \text{if deviation in } y_r(\ell) \text{ must be limited } (\ell : 1, \ldots, m-q) \tag{15}$$

$$\mathbf{e}_{us}(1) \le \beta, \quad \text{if deviation in } u_s(1) \text{ must be limited } (1 : 1, \ldots, q) \tag{16}$$

$$Re\left(\lambda_i\left\{\mathbf{G}_s\left(\mathbf{C}_i^{cv}, \mathbf{C}_i^{mv}\right)\left[\mathbf{G}_s\left(\mathbf{C}_i^{cv}, \mathbf{C}_i^{mv}\right) \otimes I_q\right]^{-1}\right\}\right) > 0, \quad \text{with } i : 1, \ldots, q \tag{17}$$

$$\det\left(\mathbf{G}_s\left(\mathbf{c}_i^{cv}, \mathbf{c}_i^{mv}\right)\right) \neq 0 \tag{18}$$

where $\|.\|_1$ represents the 1-norm, i.e. the sum of the elements of the corresponding vector. The constraints of Eqs. (13), (14) and (18) guarantee that the optimal selection of q CVs and q MVs is feasible. The inequality in Eq. (17) corresponds to the stability criterion developed in Ref. [25] for control structures designed in the context of IMC theory. Here, $Re[.]$ is the real part function, λ_i is the i-th eigenvalue, $\otimes$ denotes the element-by-element product, and I_q is the $q \times q$ identity matrix. In addition, $\mathbf{G}_s$ is rearranged so that the selected components corresponding to input–output (CVs–MVs) pairings are positioned on the diagonal. At this point, the optimal CVs–MVs pairing can be automatically obtained through the algorithms presented in Ref. [22]. On the other hand, Eqs. (15)–(16) only apply to certain UVs and specific selected MVs, respectively. Typical reference values for setting α and β arise from the obtained deviations corresponding to a preliminary design in which q is selected as $q = \min(m,n)$ (maximum order structure).

Once the *NC* is obtained, then for the *RC* design the faults scenario proposed in Section 2.3 is taken into account. Assuming that a fault could be present in the actuator j, then the corresponding gene $c_i^{mv}(j)$ in the chromosome $\mathbf{C}_i^{mv}$ must be set to 0. Similarly, $c_i^{cv}(k)$ from $\mathbf{C}_i^{cv}$ must be set to 0 if a fault could be present in the sensor of CV k. In this context, the following additional constraints must be considered for *RC* design:

$$\mathbf{C}_i^{mv}(j) = 0, \quad \text{if actuator } j \text{ is supposed to fail } (j : 1, \ldots, q) \tag{19}$$

$$\mathbf{C}_i^{cv}(k) = 0, \quad \text{if sensor } k \text{ is supposed to fail } (k : 1, \ldots, q) \tag{20}$$

These constraints can be combined, allowing to design FTC structures capable of handling multiple faults in actuators/sensors.

On the other hand, for the particular case in which $n > m$ and $q = m$, Eqs. (12)–(20) can be used for design purposes replacing only the cost function in Eq. (12) by the $\left\|\mathbf{e}_{us}(\mathbf{C}_i^{cv}, \mathbf{C}_i^{mv})\right\|_1$ performance criteria.

Finally, for those solutions that do not satisfy Eqs. (13)–(20) (unfeasible solutions) it was assigned an infinite value to the functional cost. In the context of GA, it is very likely that these solutions are discarded and are not taken into account for the next generation. Thus, the algorithm evolves towards the optimal solution reducing the percentage of unfeasible solutions during the searching process, as shown in Fig. 3b in Ref. [22].

2.4.1. *Overall procedure*

The proposed procedure can be summarized as follows:

1. Define the nominal controller (*NC*):
   - a. Select q, the dimension of the control structure as $q = \min(m,n)$.
   - b. Execute the GA based on the chromosome of Eq. (9) to find a solution which minimizes Eq. (12) subject to the constraints of Eqs. (13)–(18). Internally, the GA obtains the optimal CVs–MVs pairing based on the algorithms discussed in Ref. [22]. This allows to rearrange $\mathbf{G}_s$ in order to check the inequality of Eq. (17).
   - c. Set $q = q - 1$ and return to step 1.b. This process ends with the selection of $q = q_0$, being q_0 the minimum number of outputs that must be controlled due to the process requirements.

Steps 1.a. to 1.c. produce a set of square control structures (of different dimension). The final *NC* must be selected by trading-off the dimension and performance, which is analyzed based on the steady-state deviations of the UVs and MVs, as will be shown in Section 3.3.1.

2. Define the reconfigurable controller (*RC*):

Assuming that a *NC* of dimension $q_n \times q_n$ was selected in step 1, the faults scenario must be defined. The *RC* consists of a set of control structures RC_i which individually handles each considered fault F_i. The RC_i can be designed through the following procedure:

- a. Select q as $q = q_n$.
- b. As in step 1.b., execute the GA to solve the problem in Eq. (12) subject to Eqs. (13)–(18) and the additional constraints Eqs. (19)–(20).
- c. If the performance of the $q \times q$ structure results not acceptable, then set $q = q + 1$ and return to step 2.b. This is possible only if there is availability of degrees of freedom.

Based on the steady-state deviations of the UVs and MVs, it can be decided whether to implement or not a certain structure RC_i. In some cases, the *NC* structure can tolerate certain faults without implementing reconfiguration actions.

Note that this sequential procedure might generate suboptimal solutions for RC, because its design depends on the initial selection of the NC. However, a simultaneous selection of NC and RC might probably result in a suboptimal NC, with degraded performance. This is not acceptable on the assumption that the process will be controlled with the NC structure most of the time.

The proposed NC and RC are decentralized and can be implemented through single-input single-output (SISO) PID (proportional/integral/derivative) control loops. This type of controller is prevalent in the industry because it is the most straightforward of the control structures [31].

The following Section 2.5 describes the switching procedure which allows to implement a smooth reconfiguration from NC to the appropriate RC_i, as will be shown in Section 4.

2.5. Reconfiguration mechanism

When switching from NC to a predesigned RC_i online, the difference between the two controller outputs must be minimized in order to avoid introducing significant transients [14]. The suggested RM is illustrated in Fig. 5a–b and contemplates the following two typical cases. Here, the controller reconfiguration time t_{RC} represents the time of fault occurrence t_F plus the fault estimation time t_{FDD}, i.e. $t_{RC} = t_F + t_{FDD}$.

1. Commute to an alternative output (switch from loop $MV_a - CV_a$ to loop $MV_a - CV_b$):
   - For $t < t_{RC}$, MV_a copies MV_1 (switch in position 1). The controller PI_1 is in auto mode (it controls CV_a through MV_1) and the controller PI_2 is in manual mode (PI_2 output is set to zero, MV_2 copies MV1, and SP_b tracks CV_b).
   - At $t = t_{RC}$, the structure commutes and MV_a copies MV_2 (switch to position 2). The controller PI_1 switches to manual mode (MV_1 remains fixed) and the controller PI_2 switches to auto mode (it controls CV_b through MV_2). Note that MV_2 remains constant at the last value of MV_1 (bumpless switchover of MV_a) until SP_b is changed or CV_b changes. Finally, SP_b must be smoothly adjusted (for example through a ramp) to the required value.
2. Commute to an alternative input (switch from loop $MV_a - CV_a$ to loop $MV_b - CV_a$):
   - For $t < t_{RC}$, the controller PI_1 is in auto mode (it controls CV_a through MV_a) and the controller PI_2 is in manual mode (PI_2 output is set to zero, MV_b is set to its nominal operating value, and SP_b tracks CV_a).
   - At $t = t_{RC}$, the controller PI_1 switches to manual mode (MV_a remains fixed) and the controller PI_2 switches to auto mode (it controls CV_a through MV_b). Note that MV_b remains constant until SP_b is changed or CV_a changes. Then, SP_b must be smoothly adjusted to the required value. If necessary, the controller PI_1 output can be set to zero (through a ramp) to set MV_a to its nominal operating value.

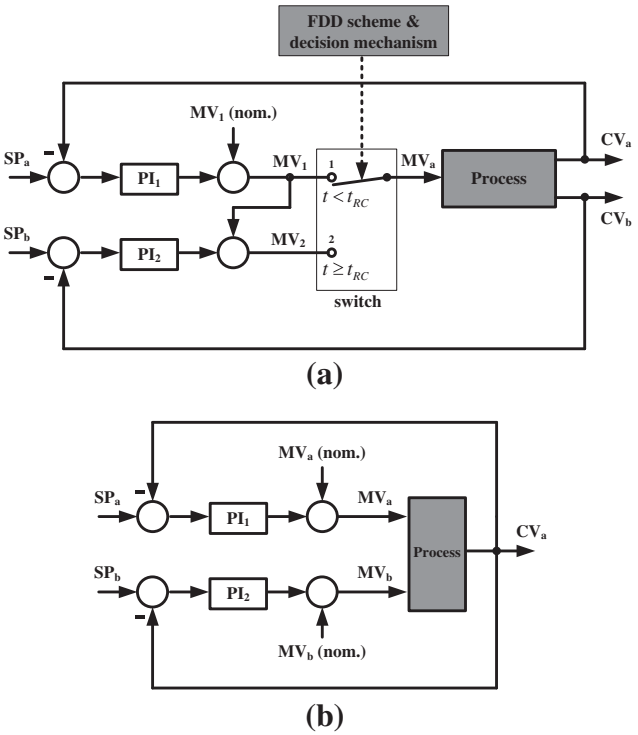

Fig. 5 – Reconfiguration mechanism: (a) switch to an alternative output, (b) switch to an alternative input.

2.6. Performance criteria

In order to demonstrate the potentiality of the approach, the closed-loop dynamic response of the FTC system when expected faults occur, and during the recovery period can be evaluated. For this purpose, the following measures are proposed:

1. Integral absolute error (IAE):

$$IAE = \int_{t_F}^{t_{final}} |e(t)|dt \tag{21}$$

where

$$e(t) = r(t) - y(t) \tag{22}$$

Here, $r(t)$ represents the setpoint, and $y(t)$ denotes the system output. In addition, t_{final} corresponds to the end of the evaluation period.

2. Error improvement percent (EIP):

$$EIP = \frac{IAE^{base} - IAE^{new}}{IAE^{base}} 100 \tag{23}$$

where *base* refers to a control structure proposed as reference, and *new* denotes a developed structure to be evaluated. The EIP index can be obtained for each output. The *new* control strategy is better than the *base* one if the EIP index results positive.

3. Maximum value of $e(t)$:

$$e_{max} = \max_{t_F \le t \le t_{final}} [e(t)] \tag{24}$$

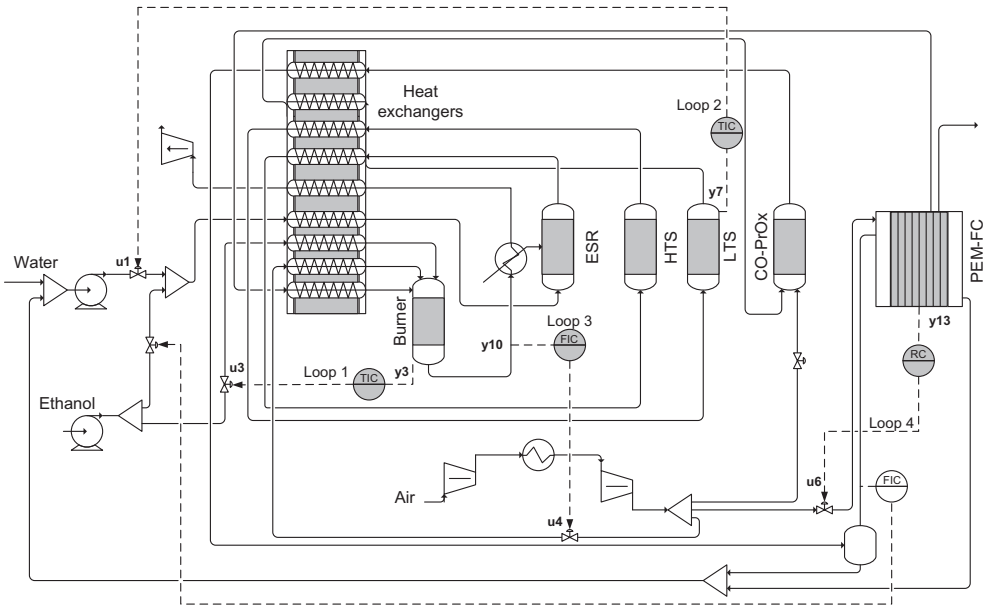

Fig. 6 – The BPS with FC. Schematic diagram and nominal controller.

4. Control energy:

$$E_u = \int_{t_F}^{t_{final}} [u(t) - u_0]^2 dt \tag{25}$$

where $u(t)$ is the control signal, and u_0 the corresponding nominal value. The E_u index can be calculated for each input.

3. FTC design for hydrogen production from bio-ethanol

The complete methodology for FTC design described in Section 2 is applied to the BPS with PEM FC presented in Ref. [29].

3.1. Description

A simplified flow sheet of the BPS is shown in Fig. 6. Most ethanol conversion to H_2 is made in the bio-Ethanol Steam Reforming (ESR) plug flow reactor. Carbon monoxide is produced in the ESR which poisons the FC catalyst. Thus, additional processing is required in order to remove this substance. The cleaning system consists of two water gas shift reactors (one of high temperature, HTS, and the other of low temperature, LTS) which favors the equilibrium of the reaction to higher conversion rates of CO. Also, a preferential oxidation of carbon monoxide (CO-PrOx) reactor is needed where oxidation of CO into CO_2 is made. A complete description of the BPS can be found in Ref. [29].

The main process requirements are [29]:

- to maintain H_2 levels on the anode of the FC;
- to maintain low the CO levels of the anode inlet stream;
- to keep the temperatures of the reactors set and FC at their operational points;
- to maintain the system efficiency.

3.2. Initial considerations

The BPS with PEM FC process is open-loop unstable. Therefore, the primary control loops presented in Ref. [32] are implemented here to stabilize the plant. The complete list of process variables is available in Table 1, where the five stabilizing control loops are indicated with (*) and the respective letter.

Following the steps showed in Fig. 1, a steady-state model and also simplified dynamic linear models must be obtained through system identification techniques. Here, the identified normalized steady-state gain matrices G and D presented in Ref. [29] (fourteen outputs $y_1 - y_{14}$, six potential inputs $u_1 - u_6$, and two disturbances $d_1 - d_2$) are utilized for supporting the FTC design step. The values of G and D are given in Appendix A. These models were constructed with respect to the most efficient operating point in terms of energy consumption [29]. In this work the FTC system is only designed for this operating region, where the obtained local models are valid. This is because most CVs and MVs do not change significantly when the control reconfiguration is executed, as will be shown in Section 4.

3.3. Controller design

3.3.1. Nominal controller (fault-free operation)

Following the design procedure, it is necessary to define a square decentralized structure for normal operation, which considers a minimum number of CVs and MVs to satisfy the objectives outlined in Section 2.1. Basic restrictions for this design are:

- to consider $q < 6$ because smaller square control structures (5×5, 4×4, etc.) respect to the 6×6 presented in Ref. [32] are attractive. In that work, all degrees of freedom (MVs) were utilized.
- y_{10} and y_{13} must be controlled. Their corresponding set-points must be modified according to the disturbance profile

Table 1 – BPS + FC process variables.

Output	Description	Input	Description
y_1	ESR exit temperature	u_1	Water to ESR inlet
y_2	Jacket exit gases temperature	u_2	Exchanged heat Q
y_3	Burner exit temperature	u_3	Ethanol to Burner
y_4	Burner entering molar flow	u_4	Oxygen to Burner
y_5	Molar ratio H_2O/Ethanol	u_5	Oxygen to CO-PrOx
y_6	HTS exit temperature	u_6	CM voltage
y_7	LTS exit temperature	u_7	ESR exit flow (*a)
y_8	CO-PrOx exit temperature	u_8	HTS exit flow (*b)
y_9	Molar ratio O_2/CO	u_9	LTS exit flow (*c)
y_{10}	Burner exit molar flow	u_{10}	CO-PrOx exit flow (*d)
y_{11}	CO-PrOx CO exit concentration	u_{11}	Bio-ethanol flow (*e)
y_{12}	Net Power		
y_{13}	Oxygen excess		
y_{14}	Stack voltage		
y_{15}	ESR pressure (*a)		
y_{16}	HTS pressure (*b)		
y_{17}	LTS pressure (*c)		
y_{18}	CO-PrOx pressure (*d)		
y_{19}	H_2 production rate (*e)		

(d_2, the stack current) in order to avoid a system efficiency loss [32].

- to consider only d_2 (the stack current) as the main disturbance. The d_1 (the ethanol purity) results not interesting for the current study [32].

In this context, the problem is to select $q-2$ CVs from a total of $14-2=12$ available measurements, and q MVs from 6 available inputs, together with the $q \times q$ CVs–MVs pairing, being $q = 5$, 4, 3, etc. Therefore, the problem to solve is:

$$\min_{(\mathbf{C}_i^*)} \left\| \mathbf{e}_{yr}(\mathbf{C}_i^*) \right\|_1 \tag{26}$$

subject to:

$$\mathbf{C}_i^* = \left[\mathbf{C}_i^{cv}(1:9), 1, \mathbf{C}_i^{cv}(10:11), 1, \mathbf{C}_i^{cv}(12), \mathbf{C}_i^{mv}(1:6) \right] \tag{27}$$

$$\sum_{k=1}^{12} \mathbf{C}_i^{cv}(k) = q-2 \tag{28}$$

$$\sum_{j=1}^{6} \mathbf{C}_i^{mv}(j) = q \tag{29}$$

$$Re\left(\lambda_i \left\{ \mathbf{G}_s(\mathbf{C}_i^*) \left[\mathbf{G}_s(\mathbf{C}_i^*) \otimes I_q \right]^{-1} \right\} \right) > 0, \quad \text{with } i: 1, \ldots, q \tag{30}$$

$$\det\left(\mathbf{G}_s(\mathbf{C}_i^*) \right) \neq 0 \tag{31}$$

where $\mathbf{C}_i^*$ represents the searched chromosome which has a length of 20 (binary) genes, i.e. 14 decision variables for the CVs (corresponding to y_1 to y_{14}) and 6 decision variables for the MVs (u_1 to u_6), see Table 1. When the value of a gene is forced to be 1, this means that the corresponding variable will always be selected by the GA for control purposes. On the other hand, when it is forced to be 0 this implies the opposite situation. As an example, consider the following components of $\mathbf{C}_i^*$ in Eq. (27) (Eq. (32) and Table 6 can be analyzed in the same way):

1. $\mathbf{c}_i^{cv}(1:9)$ contains the genes corresponding to y_1 to y_9. They can individually take values of 0 or 1 along the GA execution, i.e. they are not fixed.
2. the next component "1" represents the value of the gene corresponding to y_{10}. It is forced to be 1, i.e. the output y_{10} is forced to be selected as a CV (this selection will not change along the GA execution).
3. $\mathbf{C}_i^{cv}(10:11)$ contains the genes corresponding to y_{11} and y_{12}. Idem to item 1.
4. the next component "1": represents the value of the gene corresponding to y_{13}. Idem to item 2.
5. $\mathbf{C}_i^{cv}(12)$ contains the gene corresponding to y_{14}. Idem to item 1.
6. $\mathbf{C}_i^{mv}(1:6)$ contains the genes corresponding to u_1 to u_6. They can individually take values 0 or 1 along the GA execution, i.e. they are not fixed.

The GA was executed 4 times ($q = 6,5,4,3$) with the settings shown in Table 2. Four alternative NC were obtained: NC_0 (6×6), NC_1 (5×5), NC_2 (4×4) and NC_3 (3×3). Table 3 presents the optimal solutions corresponding to each selected q. The optimal pairing between the CVs and MVs was systematically obtained through the branch a bound (BAB) solution proposed in Ref. [33]. This BAB method utilizes a biobjective selection criteria based on the relative gain array and the μ-interaction measure. This algorithm results computationally efficient for the BPS with FC process ($n = 6$). In addition, Table 4 shows the obtained steady-state deviations of the most important UVs and MVs (the components of $\mathbf{e}_{yr}$ and $\mathbf{e}_{us}$, respectively).

The obtained NC_0 (6×6) is equivalent to the control structure presented in Ref. [32]. Considering the obtained deviations (Table 4), the NC_1 (5×5) does not suggest a noticeable performance deterioration with respect to NC_0. Additionally, excessive control energy requirements are not expected. However, NC_1 only reduces the dimension of the structure in 1 loop. On the other hand, NC_2 and NC_3 foresee a performance degradation in the CO-PrOx CO exit concentration (y_{11}). Then, in order to minimize this deviation, the problem of Eq. (26) was solved by updating Eq. (27) as:

Table 2 – Genetic algorithm parameters.

N_i (initial population)	N_c (chromosome length)	N_g (no. of generations)	Mutation probability	Crossover probability	Selection method
10,000	20	50	$0.7/N_c$	0.7	Roulette wheel

Table 3 – Decentralized nominal controllers. Alternative solutions.

	NC_0	NC_1	NC_2	NC_3	NC_4
q:	6	5	4	3	4
	$u_2 - y_1$	$u_3 - y_3$	$u_3 - y_3$	$u_3 - y_3$	$u_3 - y_3$
	$u_3 - y_3$	$u_5 - y_8$	$u_5 - y_8$	$u_4 - y_{10}$	$u_1 - y_7$
	$u_5 - y_8$	$u_1 - y_9$	$u_4 - y_{10}$	$u_6 - y_{13}$	$u_4 - y_{10}$
	$u_1 - y_9$	$u_4 - y_{10}$	$u_6 - y_{13}$		$u_6 - y_{13}$
	$u_4 - y_{10}$	$u_6 - y_{13}$			
	$u_6 - y_{13}$				

$$\mathbf{C}_i^* = \left[\mathbf{C}_i^{cv}(1:2), 1, \mathbf{C}_i^{cv}(3:8), 1, 0, \mathbf{C}_i^{cv}(9), 1, \mathbf{C}_i^{cv}(10), \mathbf{C}_i^{mv}(1:6)\right] \tag{32}$$

and adding the following constraint (see Eq. (15)):

$$\mathbf{e}_{yr}(11) \leq 0.26 \tag{33}$$

The proposed limitation value in Eq. (33) arises from the obtained deviation in y_{11} corresponding to the maximum order structure NC_0 (see Table 4). The fixed 0 in $\mathbf{C}_i^*(11)$ indicates that y_{11} is not controlled. It is not convenient to control y_{11} because:

- to measure concentrations is expensive, it can introduce time delay, and it is not performed in most of the plants,
- it is not optimal from a plantwide perspective in this process.

On the other hand, the fixed 1 in $\mathbf{C}_i^*(3)$ indicates that y_3 is controlled (in addition to y_{10} and y_{13}). In this case it was observed that it is impossible to minimize the deviation $\mathbf{e}_{yr}(3)$ otherwise. Thus, the GA was executed again with $q = 4$ and the above constraints (Eqs. (32) and (33)). The NC_4 (4×4) was obtained (see Tables 3 and 4).

Comparing NC_4 against NC_1 from Table 4, it is expected that:

Table 4 – Alternative nominal controllers. Steady-state deviations of each UV and MV.

	NC_0 (6×6)	NC_1 (5×5)	NC_2 (4×4)	NC_3 (3×3)	NC_4 (4×4)
y_1	–	0.13	0.12	0.12	0.15
y_3	–	–	–	–	–
y_7	0.62	0.58	0.79	0.79	–
y_8	–	–	–	0.11	2.70
y_9	–	–	1.29	0.86	0.85
y_{10}	–	–	–	–	–
y_{11}	0.26	0.21	0.34	0.31	0.20
y_{12}	0.64	0.63	0.59	0.59	0.62
y_{13}	–	–	–	–	–
u_1	1.45	1.49	–	–	2.92
u_2	1.30	–	–	–	–
u_3	3.91	4.00	4.21	4.24	4.04
u_4	0.96	0.96	0.89	0.89	1.04
u_5	11.40	11.22	8.59	–	–
u_6	2.34	2.34	2.34	2.34	2.34

- y_{11} will not deteriorate its performance.
- y_8 and y_9 will deteriorate their performance.
- u_1 will require more control energy.

The potentiality of this analysis based on the individual squared deviations of the UVs and the MVs is demonstrated in Section 4. The advantage of NC_4 is that it reduces the dimension of the structure in 2 loops. As concluded in Section 4.1, the NC_4 will be finally selected as the NC structure due to the good trade-off between its dimension and overall performance. It is shown in Fig. 6 where the proposed controllers are highlighted with gray background.

Finally, it is not possible to reduce NC_4 dimension to 3×3 because to control y_3, y_{10} and y_{13} is necessary, but not sufficient.

3.3.2. *Reconfigurable controller*

An optimal reduced control structure for normal operation (NC_4) which only considers 4 CVs and 4 MVs was presented above in Section 3.3.1. It ensures availability of redundancies because u_2 and u_5 represent extra degrees of freedom for FTC design.

According to Section 2.3, typical faults in the process components are considered and summarized in Table 5. For these faults, common restrictions for the design are:

- for F_1 to F_4, all inputs (u_1 to u_6) are taken into account for the design, except the faulty actuator related to F_j (for which $\mathbf{C}_i^{mv}(j) = 0$). For F_5 to F_8 this restriction does not apply, and all MVs can be considered.
- for F_5 to F_8, all sensors are taken into account for the design, except the faulty sensor related to F_k (for which $\mathbf{C}_i^{cv}(k) = 0$). For F_1 to F_4 this restriction does not apply, and all outputs can be considered.
- q is initially set to be 4. If the performance of the resulting 4×4 structure is not acceptable, then q can be set to be 5. For F_5 to F_8, $q = 6$ is also possible (all inputs can be selected as MVs).
- As proposed in Section 3.3.1, y_{11} is not controlled. This allows to evaluate and minimize $\mathbf{e}_{yr}(11)$. Again, the search is driven to have $\mathbf{e}_{yr}(11) \leq 0.26$.

For each fault scenario, the GA is executed with the settings shown in Table 2 to solve the problem in Eq. (12) subject to Eqs. (13)–(20) and the specific chromosomes presented in Table 6. The corresponding chromosome for F_1 indicates that the measurements y_3, y_{10} and y_{13} are CVs. On the other hand,

Table 5 – Proposed faults.

Fault	Variable definition	Type	Value
F_1	Water to ESR actuator (u_1)	Blockade	+5%
F_2	Ethanol to burner actuator (u_3)	Blockade	−5%
F_3	Oxygen to burner actuator (u_4)	Blockade	+5%
F_4	CM voltage actuator (u_6)	Blockade	−5%
F_5	LTS exit temp. sensor (y_7)	Complete loss	
F_6	Burner exit temp. sensor (y_3)	Complete loss	
F_7	Burner exit molar flow sensor (y_{10})	Complete loss	
F_8	Oxygen excess sensor (y_{13})	Complete loss	

Table 6 – Reconfigurable controller design. GA chromosomes for each fault.

Fault	Chromosome
F_1	$C_i^* = [C_i^{cv}(1:2), 1, C_i^{cv}(3:8), 1, 0, C_i^{cv}(9), 1, C_i^{cv}(10), 0, C_i^{mv}(1:5)]$
F_2	$C_i^* = [C_i^{cv}(1:10), 0, C_i^{cv}(11:13), C_i^{mv}(1:2), 0, C_i^{mv}(3:5)]$
F_3	$C_i^* = [C_i^{cv}(1:10), 0, C_i^{cv}(11), 1, C_i^{cv}(12), C_i^{mv}(1:3), 0, C_i^{mv}(4:5)]$
F_4	$C_i^* = [C_i^{cv}(1:9), 1, 0, C_i^{cv}(10:12), C_i^{mv}(1:5), 0]$
F_5	$C_i^* = [C_i^{cv}(1:6), 0, C_i^{cv}(7:8), 1, 0, C_i^{cv}(9), 1, C_i^{cv}(10), C_i^{mv}(1:6)]$
F_6	$C_i^* = [C_i^{cv}(1:2), 0, C_i^{cv}(3:9), 0, C_i^{cv}(10:12), C_i^{mv}(1:6)]$
F_7	$C_i^* = [C_i^{cv}(1:9), 0, 0, C_i^{cv}(10:12), C_i^{mv}(1:6)]$
F_8	$C_i^* = [C_i^{cv}(1:10), 0, C_i^{cv}(11), 0, C_i^{cv}(12), C_i^{mv}(1:6)]$

Table 7 – Decentralized reconfigurable controllers.

Controller/Fault:	RC_1/F_1	RC_1'/F_1	RC_2/F_2	RC_3/F_3	RC_4/F_4
q:	4	5	4	4	4
	$u_3 - y_3$ $u_5 - y_9$ $u_4 - y_{10}$ $u_6 - y_{13}$	$u_2 - y_1$ $u_3 - y_3$ $u_5 - y_9$ $u_4 - y_{10}$ $u_6 - y_{13}$	$u_2 - y_1$ $u_5 - y_8$ $u_1 - y_9$ $u_6 - y_{13}$	$u_3 - y_3$ $u_5 - y_8$ $u_1 - y_9$ $u_6 - y_{13}$	$u_3 - y_3$ $u_5 - y_8$ $u_1 - y_9$ $u_4 - y_{10}$
Controller/Fault:	RC_5/F_5	RC_6/F_6	RC_7/F_7	RC_8/F_8	
q:	5	4	4	4	
	$u_3 - y_3$ $u_5 - y_8$ $u_1 - y_9$ $u_4 - y_{10}$ $u_6 - y_{13}$	$u_2 - y_1$ $u_5 - y_8$ $u_1 - y_9$ $u_6 - y_{13}$	$u_3 - y_3$ $u_5 - y_8$ $u_1 - y_9$ $u_6 - y_{13}$	$u_3 - y_3$ $u_5 - y_8$ $u_1 - y_9$ $u_4 - y_{10}$	

F_2 and F_5 represent a complicated scenario for the y_3 dynamics. For F_2, it was necessary to relax the restriction which defines y_{10} and y_{13} as CVs because it was not found another alternative to reduce the deviation in y_3. For F_3, the restriction corresponding to y_{10} is relaxed. It is not known a priori if y_{10} can be controlled with a MV different from u_4. The same situation occurs for F_4 with y_{13} and u_6. Finally, the proposed chromosome for F_6 implies that the restrictions associated with y_{10} and y_{13} are relaxed.

The obtained RC_i corresponding to each faulty case are presented in Table 7. The obtained steady-state deviations of the most important UVs and MVs are showed in Table 10 in Appendix B. In addition, Table 11 in Appendix C presents the steady-state deviations associated to several 3×3 structures obtained from NC_4 when each particular fault F_i affects the system (the control loop corresponding to each faulty component does not work). Through analysis and comparison of the results of Tables 4, 10 and 11, the principal expected characteristics of each RC_i are summarized in Table 8.

The dimension of RC_1 results 4×4. It introduces the loop $u_5 - y_9$ so as to reconfigure NC_4 subject to F_1. For this case, an alternative structure RC_1' (5×5) was also developed. But it does not anticipate a noticeable improvement for the dynamics of y_8 and u_5 (see Table 10), even though it increases the dimension of the controller.

The dimension of RC_2 is also 4×4, but it proposes a major reconfiguration of the NC_4.

On the other hand, the developed RC_3 does not suggest to control y_{10} with an alternative MV (different from u_4). Given that no significant deterioration is anticipated for this fault F_3 (see Table 11), it was decided not to implement RC_3. The same situation occurs for F_4 with RC_4.

The disadvantage of RC_5 (5×5) is that it increases the order of the structure. However, it was not obtained a 4×4 solution for handling simultaneously the deviations in y_3 and y_8 during the design process.

Finally, the solutions RC_6, RC_7 and RC_8 (which accommodate F_6, F_7 and F_8) result identical to RC_2, RC_3 and RC_4, respectively. Again, RC_7 and RC_8 are not implemented due to the same reason given for RC_3 and RC_4.

4. Closed-loop analysis

In the following, the performance of the FTC system is dynamically evaluated through a complete set of simulations. It is done under the Urban Dynamometer Driving Schedule

Table 8 – Reconfigurable controllers. Expected characteristics based on the individual steady-state deviations.

Fault/Action	Advantages	Disadvantages
F_1/without RC_1		- decreased performance in y_7 and y_{11} (not allowed)
F_1/implementing RC_1	- y_{11} will improve its performance	- y_7 will not improve its performance - y_8 will deteriorate its performance - u_5 will require more control energy
F_2/without RC_2		- decreased performance in y_3 (not allowed)
F_2/implementing RC_2	- y_3 will improve its performance	- y_7 and y_{10} will deteriorate their performance
F_3/without RC_3		- decreased performance in y_{10}
F_3/implementing RC_3	- several outputs will improve performance	- y_7 will deteriorate its performance
F_4/without RC_4		- decreased performance in y_{13}
F_4/implementing RC_4	- several outputs will improve performance	- y_7 will deteriorate its performance
F_5/without RC_5		- decreased performance in y_7 and y_{11} (not allowed)
F_5/implementing RC_5	- y_7 and y_{11} will improve performance	

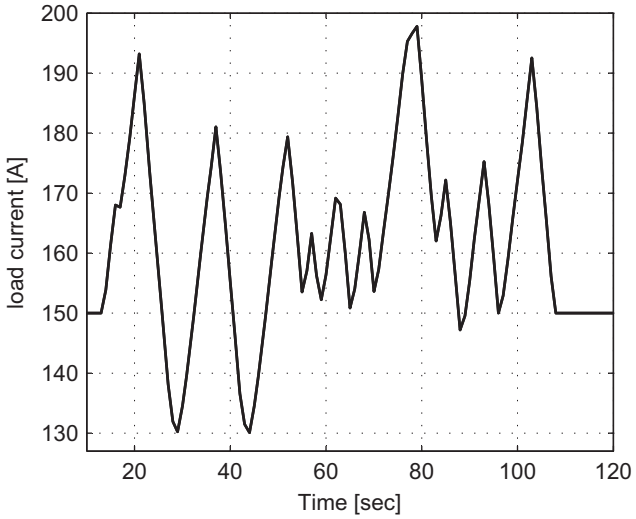

Fig. 7 – Current profile demanded to the FC.

(UDDS). This standardized profile represents a typical scenario which was stated for measuring both pollutant emissions and gasoline economy of engines [30]. The corresponding current profile demanded to the FC is shown in Fig. 7 which represents a major disturbance for the system.

Figs. 8–15 show the dynamic responses corresponding to key variables of the process. The performance of the complete FTC system is confronted with the nominal structure (the NC_4) which has no fault-tolerant capability, under different fault scenarios (see Table 5). In addition, Tables 13, 14 and 15 in Appendix E show the obtained IAE and E_u indexes.

In the simulations, the RM proposed in Section 2.5 is implemented to allow a smooth reconfiguration to the appropriate control strategy. The proposed structures are implemented via SISO PI controller type. Table 12 in Appendix D shows the selected parameters for each loop according to Refs. [34,35].

4.1. *Nominal controller performance*

Figs. 8–10 show several responses corresponding to the NC_4 structure, which is confronted with the other candidate solutions obtained in Section 3.3.1. Fig. 8a shows the dynamics of the CO-PrOx CO exit concentration (y_{11}). The NC_4 structure presents good regulatory behavior subject to the UDDS profile, with a reduction in the corresponding IAE value with respect to NC_2:$EIP(y_{11}) = 52.6\%$. Note that both NC_2 and NC_4 are 4×4 structures. As can be seen, the CO concentration with respect to NC_0 is acceptable. In Figs. 8b and 9a the ESR exit temperature (y_1) and the CO-PrOx exit temperature (y_8) responses are showed, respectively. The NC_4 strategy presents good regulatory behavior, with an acceptable increase in the e_{max} values: $e_{max}(y_1) = 0.34$ (NC_0) and $e_{max}(y_1) = 4.20$ (NC_4), and $e_{max}(y_8) = 6.00$ (NC_0) and $e_{max}(y_8) = 27.04$ (NC_4). This is because these outputs are not controlled by the NC_4 structure (see Table 3). The remaining outputs present similar dynamics, as shown in Table 13 (Appendix E). In addition, Fig. 9b depicts the suitable evolution of the water to ESR inlet (u_1) without excessive control energy requirements. This behavior is observed for all inputs, as shown in Table 13. Finally, the overall efficiency of BPS depends on the net power output (y_{12}) of the system and the total ethanol consumed in the fuel processor for burning and reforming ($u_3 + u_{11}$) [32]. Fig. 10a–b show the dynamics of these variables. As can be seen, y_{12} presents the same performance. In addition, the total ethanol consumption is also similar: $\int_{t_0}^{t_{final}} (u_3 + u_{11})dt = 56.09$ mol for NC_0, and $\int_{t_0}^{t_{final}} (u_3 + u_{11})dt = 56.03$ mol for NC_4 over the simulation time $[t_0, t_{final}]$. Therefore, NC_4 maintains the system efficiency when compared to NC_0. A justification about the behavior of the control actions is provided at the end of this section. Given the good balance between its dimension and overall performance, the NC_4 was finally proposed as the NC structure.

4.2. *Reconfigurable controller performance*

The first simulation corresponds to a fault in the water to ESR manipulated variable (u_1), called F_1. In this case a sticking at +5% with respect to the normal operating point was considered, which occurs at $t_{F1} = 18$ s. The fault estimation time (t_{FDD}) is assumed to be $t_{FDD} > 30\tau_{min}$, where τ_{min} is around 0.05 s, the smallest time constant of the plant [21].

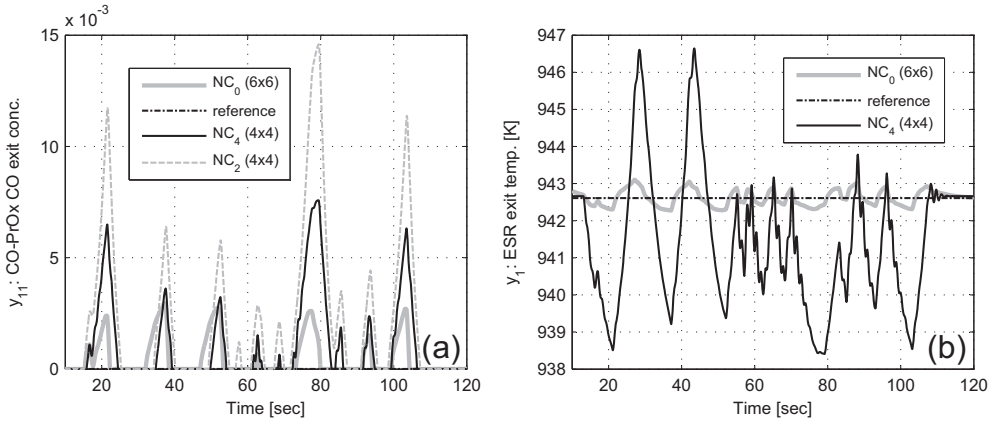

Fig. 8 – y_{11} and y_1 dynamic responses.

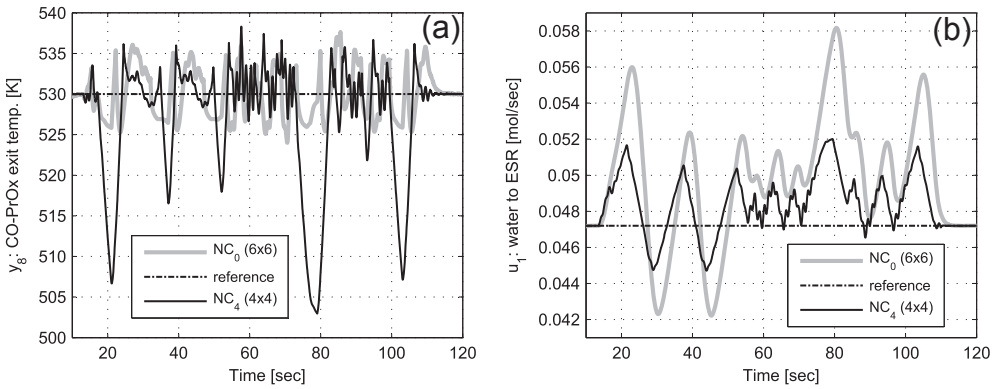

Fig. 9 – y_8 and u_1 dynamic responses.

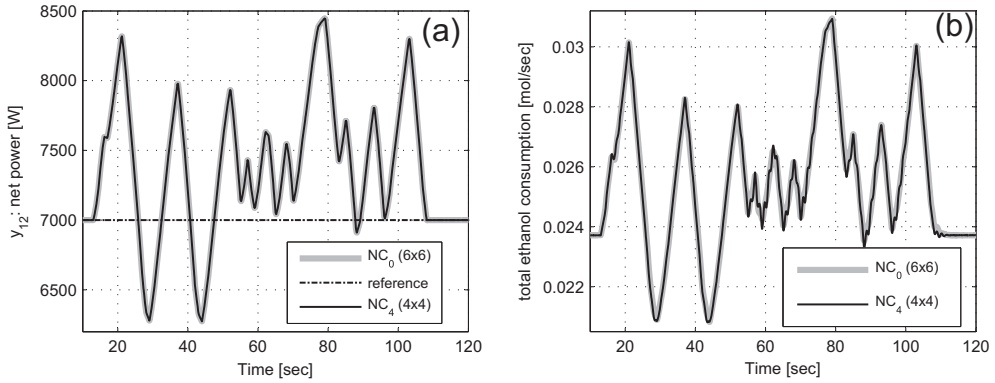

Fig. 10 – y_{12} and total ethanol consumed in the FC.

Therefore, $t_{FDD} = 1.7$ s. is adopted for all simulations. Here, the controller reconfiguration time t_{RC} results $t_{RC} = t_{F1} + t_{FDD} = 19.7$ s. Fig. 11b shows the dynamic behavior of the CO-PrOx CO exit concentration (y_{11}). The RC_1 presents good regulatory actions in presence of the UDDS profile, maintaining low the CO concentration with respect to the nominal structure (which has no fault-tolerant capability): $EIP(y_{11}) = 47.3\%$. Fig. 12a–b show the LTS exit temperature (y_7) and the CO-PrOx exit temperature (y_8) responses, respectively. The RC_1 presents an acceptable deterioration in performance with regard to the nominal NC_4, with an admissible increase in the e_{max} values: $e_{max}(y_7) = 15.7$ (NC_4) and $e_{max}(y_7) = 16.3$ (RC_1), and $e_{max}(y_8) = 26.99$ (NC_4) and $e_{max}(y_8) = 47.03$ (RC_1). The remaining outputs present good performance, with a small increase in the corresponding IAE values, as shown in Table 14. On the other hand, the molar ratio H_2O/Ethanol (u_5) presents an adequate evolution without saturations or excessive energy requirements (see Fig. 11a). The other inputs present good performance, as shown in Table 14.

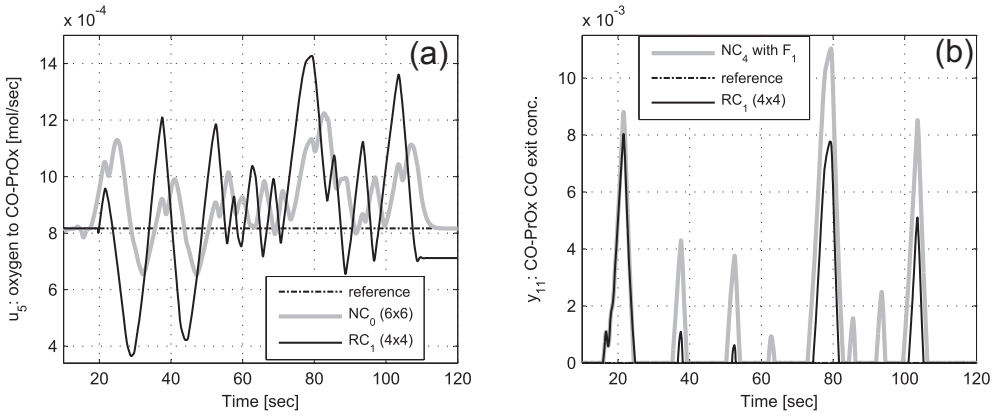

Fig. 11 – u_5 and y_{11} dynamic responses (fault F_1: water to ESR sticking at +5%).

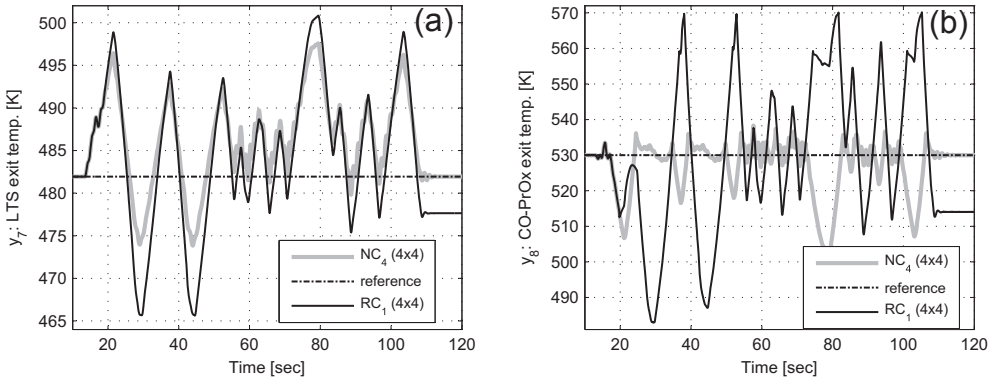

Fig. 12 – y_7 and y_8 dynamic responses (fault F_1: water to ESR sticking at +5%).

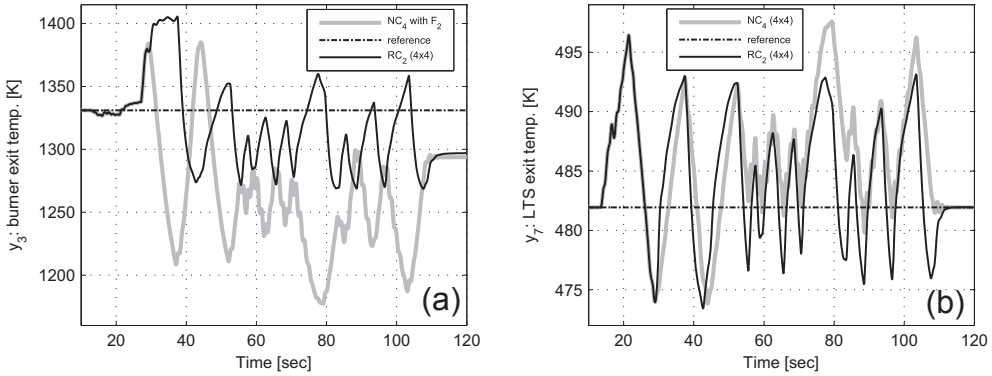

Fig. 13 – y_3 and y_7 dynamic responses (fault F_2: ethanol to burner sticking at −5%).

The second simulation case is presented in Fig. 13a–b and considers a fault in the ethanol to burner manipulated variable (u_3), called F_2. A sticking at −5% with respect to the normal operating point was considered, which occurs at $t_{F_2} = 27.1$ s. As stated above, the adopted fault estimation time is $t_{FDD} = 1.7$ s. Then, the controller reconfiguration time results $t_{RC} = 28.8$ s. Fig. 13a shows the dynamic behavior of the burner exit temperature (y_3). The IAE index is significantly improved by implementing the RC_2 structure, which maintains low the variability of y_3 with respect to the nominal structure (which has no fault-tolerant capability): $EIP(y_3) = 53.3\%$. Fig. 13b shows the LTS exit temperature (y_7) response. It presents good performance with regard to the nominal NC_4, with a decrease in the IAE value: $EIP(y_7) = 9.1\%$. On the other hand, the burner exit molar flow (y_{10}) deteriorates its performance, but this does not affect the net power output (y_{12}) of the system. Additionally, the total consumption of ethanol does not increase: $\int_{t_0}^{t_{final}} (u_3 + u_{11})dt = 56.03$ mol for NC_4, and

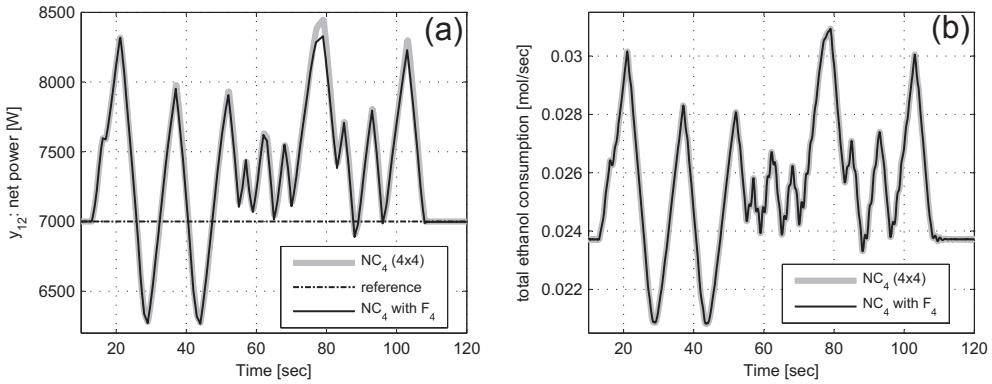

Fig. 14 – y_{12} and total ethanol consumed in the FC (fault F_4: CM voltage sticking at −5%).

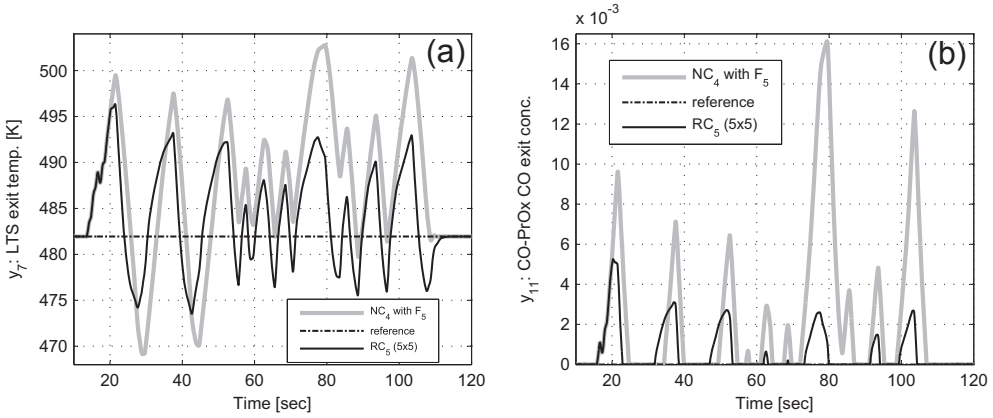

Fig. 15 – y_7 and y_{11} dynamic responses (fault F_5: LTS exit temp. sensor loss).

$\int_{t_0}^{t_{final}}(u_3+u_{11})dt = 53.79$ mol for RC_2. Therefore, RC_2 maintains the system efficiency when compared to NC_4. The remaining variables present acceptable performance, as shown in Table 14.

The third testing scenario corresponds to a fault in the oxygen to burner manipulated variable (u_4), called F_3. In this case a sticking at +5% with respect to the normal operating point was considered, which occurs at $t_{F_3} = 14.5$ s. In Section 3.3.2 it was decided not to implement any reconfiguration for this fault. As can be seen from Table 14, no significant deterioration occurs when the fault F_3 is present. Note that $e_{max}(y_1) = 4.20$ (NC_4) and $e_{max}(y_1) = 9.69$ (NC_4 affected by F_3), which represents an admissible performance. But, the burner exit molar flow (y_{10}) noticeably deteriorates its performance because it is not controlled once the fault appears. However, the net power output (y_{12}) of the system is not affected and the total consumption of ethanol does not increase. Thus the system efficiency is still maintained.

Another simulation case is presented in Fig. 14a–b and considers a fault in the compressor motor voltage manipulated variable (u_6), called F_4. A sticking at −5% with respect to the normal operating point was considered, which occurs at $t_{F_4} = 26.8$ s. Analogously to the previous case, a reconfiguration was not applied for this fault. Again, no meaningful dynamic deterioration occurs when the fault F_4 arises (see Table 14), except the oxygen excess (y_{13}) which is not controlled when F_4 appears. Only for this scenario the overall efficiency of BPS results slightly degraded. As can be seen from Fig. 14b, the total ethanol consumption is similar. But, Fig. 14a shows that the net power (y_{12}) deteriorates its performance.

On the other hand, there are no appreciable differences between the dynamics of: RC_6 and RC_2, NC_4 affected by F_7 and F_3, and NC_4 affected by F_8 and F_4, respectively. This can be seen in Tables 14 and 15, where the IAE and E_u indexes present similar values. Thus, the associated figures are not depicted here.

The fifth testing case is displayed in Fig. 15a–b and considers a fault in the LTS exit temperature sensor (y_7), called F_5. An abrupt loss of the measurement which occurs at $t_{F_5} = 18$ s. was considered. Again, the adopted fault estimation time is $t_{FDD} = 1.7$ s. Thus, the controller reconfiguration time results $t_{RC} = 19.7$ s. Fig. 15a–b show the LTS exit temperature (y_7) and the CO-PrOx CO exit concentration (y_{11}) responses, respectively. The IAE index is significantly improved by implementing the RC_5 structure, which maintains low the variability of y_{11} and y_7 when compared to the nominal structure (which has no fault-tolerant capability): $EIP(y_{11}) = 72.8\%$ and $EIP(y_7) = 37.3\%$. The remaining variables present good performance, as shown in Table 15. Finally, the net power output (y_{12}) of the system is not affected and the total consumption of ethanol does not increase: $\int_{t_0}^{t_{final}}(u_3+u_{11})dt = 56.03$ mol for NC_4, and $\int_{t_0}^{t_{final}}(u_3+u_{11})dt = 56.05$ mol for RC_5. Therefore, RC_5 keeps the system efficiency when compared to NC_4.

As shown, the proposed FTC structure maintains the overall system efficiency through different failure scenarios. On the other hand, in all cases it keeps the H_2 levels on the anode of the FC without excessive use of bio-ethanol. This is because the tracking of the H_2 production rate y_{19} (it is one of the stabilizing control loops) presents a very good performance (see Tables 13, 14 and 15 in Appendix E). It has a changing setpoint due to the hydrogen demand of the FC which varies as a function of the demanded current.

Finally, the presented structures were not designed trying to minimize explicitly the control energy expenditure (the restriction of Eq. (16) was not used). However, from the simulations (see Tables 13, 14 and 15 in Appendix E) it was verified the adequacy of the control actions. In fact, the minimization of eq. (12) implies to construct $\mathbf{G}_s$ such that its minimum singular value is increased, indicating good controllability. This means that the deviations in the MVs will not be excessive, as it was demonstrated in Appendix C in Ref. [26].

5. Conclusions and future work

A novel decentralized FTC methodology for safe production of hydrogen from bio-ethanol was presented in this work. It

was shown that a correct on-line selection between a set of pre-designed controllers can suitably handle usual faults that occur in actuators and sensors. Then, a particular PI-based control structure is implemented for each fault mode so as to ensure stability and acceptable performance. This was done through a reconfiguration mechanism which minimizes the switching transients. Several performance indexes have been considered in order to demonstrate the achievable improvements of the fault-tolerant system. The approach takes advantage of the redundancies based on the quantification of the individual steady-state squared deviations. It considers only steady-state information, trying to reduce the use of heuristic considerations. In addition, genetic algorithms propose an effective treatment for the overall problem.

If it is desired to apply the approach to other case studies, a major difficulty that might arise is the impossibility to design a nominal control structure which has a reduced dimension. This implies that extra resources will not be available to design the set of reconfigurable controllers.

The presented framework seems to indicate that the methodology could be extended to handle other type of faults, such as plant faults. The basic idea would be to construct a new steady-state model which takes into account the abnormal behavior of the process. Then, the model can be utilized to design the corresponding reconfigurable controller, as described in Section 2.4. Considering this, some process faults such as those proposed in Ref. [36] could be analyzed through the presented approach. Moreover, the abnormal events acting in sequential form, and also simultaneously could be evaluated.

On the other hand, the problem of redundancies selection will be considered so as to reduce the number of additional actuators and sensors to be installed. Usually this issue is not addressed because the tendency is to use all the available control freedom, i.e. an explicit analysis of the system redundancy is not performed.

Finally, future work will be focused on integrate the developed FTC system to the FDD scheme proposed in Ref. [36]. Also, a large-scale case which includes the heat exchanger network model will be addressed too.

Acknowledgments

The authors thank the financial supports from ANPCyT (Agencia Nacional de Promoción Científica y Técnica), UNR-FCEIA (Universidad Nacional de Rosario) and CONICET (Consejo Nacional de Investigaciones Científicas y Técnicas). The authors also acknowledge the support from UTN-FRRo (Universidad Tecnológica Nacional) and CAPEG-CIFASIS (Computer Aided Process Engineering Group).

Nomenclature

BPS	bio-ethanol processor system
CV	controlled variable
FC	fuel cell
FDD	fault detection and diagnosis
FTC	fault-tolerant control
GA	genetic algorithm
MV	manipulated variable
NC	nominal controller
PEM	proton exchange membrane
RC	reconfigurable controller
RM	reconfiguration mechanism
t_F	time of fault occurrence
t_{FDD}	fault estimation time
t_{RC}	controller reconfiguration time
UDDS	Urban Dynamometer Driving Schedule
UV	uncontrolled variable

Appendix A

Table 9 – BPS + FC normalized steady-state gains.

	G						D	
	u_1	u_2	u_3	u_4	u_5	u_6	d_1	d_2
y_1	−0.0012	0.9250	0.0157	0.1658	0.0030	−0.0189	−0.0021	−0.2811
y_2	0.1397	−0.5491	0.0615	0.6641	−0.0040	−0.0015	−0.0036	−0.7037
y_3	−0.2998	−0.2600	0.5627	−0.6554	0.0071	−0.0046	0.3538	0.4096
y_4	0.5028	−0.0852	0.0020	−0.0167	0.0541	−0.0060	−0.0724	0.7594
y_5	0.6500	0.1728	0.0080	0.0236	−0.0058	−0.0040	0.2533	−0.7062
y_6	−0.6530	0.6671	0.0046	0.1194	−0.0009	0.0087	0.0966	−0.1923
y_7	−0.7799	0.0793	0.0004	0.0169	0.0056	0.0070	0.1078	0.8877
y_8	−0.9448	−0.0536	−0.1032	0.1095	0.3593	0.1900	0.3286	−0.0847
y_9	0.7183	0.0184	0.0024	−0.0139	0.1876	−0.0125	−0.1250	−0.9165
y_{10}	0.2080	−0.0347	0.0888	0.9650	0.0023	−0.0013	−0.0048	0.0400
y_{11}	−0.2903	0.1212	0.0856	−0.0709	−0.0680	−0.1415	−0.1304	0.6714
y_{12}	0.0115	0.0167	0.0045	−0.0018	0.0066	−0.0609	0.0087	0.8192
y_{13}	−0.0027	0.0005	0.0001	0.0013	0.0020	0.7526	−0.0010	−0.5717
y_{14}	0.0017	0.0062	0.0017	−0.0026	0.0003	0.4741	0.0031	−0.8188

Appendix B

Table 10 – Reconfigurable controllers. Steady-state deviations of each UV and MV.

	RC_1	RC_1'	RC_2	RC_3	RC_4	RC_5	RC_6	RC_7	RC_8
y_1	0.11	–	–	0.08	0.12	0.13	–	0.08	0.12
y_3	–	–	0.15	–	–	–	0.15	–	–
y_7	0.84	0.90	0.64	0.58	0.60	0.58	0.64	0.58	0.60
y_8	7.47	7.33	–	–	–	–	–	–	–
y_9	–	–	–	–	–	–	–	–	–
y_{10}	–	–	0.07	0.10	–	–	0.07	0.10	–
y_{11}	0.22	0.26	0.26	0.21	0.22	0.21	0.26	0.21	0.22
y_{12}	0.65	0.66	0.64	0.63	0.70	0.63	0.64	0.63	0.70
y_{13}	–	–	–	–	0.32	–	–	–	0.32
u_1	–	–	1.48	1.49	1.37	1.49	1.48	1.49	1.37
u_2	–	1.28	1.26	–	–	–	1.26	–	–
u_3	4.35	4.21	–	3.32	4.02	4.00	–	3.32	4.02
u_4	0.89	0.90	–	–	0.96	0.96	–	–	0.96
u_5	52.90	52.61	11.30	11.27	11.90	11.22	11.30	11.27	11.90
u_6	2.32	2.32	2.34	2.34	–	2.34	2.34	2.34	–

Appendix C

Table 11 – Steady-state deviations corresponding to NC_4 affected by each fault F_i.

	F_1, F_5	F_2, F_6	F_3, F_7	F_4, F_8
y_1	0.12	0.15	0.09	0.14
y_3	–	0.57	–	–
y_7	0.79	–	–	–
y_8	0.11	2.68	2.75	2.94
y_9	0.86	0.85	0.86	0.85
y_{10}	–	–	0.20	–
y_{11}	0.31	0.23	0.20	0.23
y_{12}	0.59	0.62	0.62	0.69
y_{13}	–	–	–	0.33
u_1	–	2.92	2.95	2.91
u_2	–	–	–	–
u_3	4.24	–	3.63	4.05
u_4	0.89	1.22	–	1.04
u_5	–	–	–	–
u_6	2.34	2.34	2.34	–

Appendix D

Table 12 – SISO PI controller parameters for each loop.

MV	CV	K_c	T_i
u_1	y_9	0.005	2.671
u_1	y_7	−0.11	0.23
u_2	y_1	0.039	3.327
u_3	y_3	4.5×10^{-5}	0.055
u_4	y_{10}	0.001	0.047
u_5	y_8	1×10^{-6}	0.05
u_5	y_9	2.8	0.001
u_6	y_{13}	5.071	0.140

Appendix E

Table 13 – Dynamic performance comparison. IAE and E_u values corresponding to alternative nominal controllers.

	NC_0	NC_1	NC_2	NC_3	NC_4
y_1	396.9	3589.3	4026.7	4006.1	3785.6
y_3	7030.2	6308.2	4414.0	4470.0	6096.4
y_7	9926.4	9789.1	16,724.4	16,706.8	11,273.6
y_8	5754.5	5723.2	5138.1	13,207.1	10,455.9
y_9	1428.6	1421.2	1801.5	1744.5	1306.5
y_{10}	6.13	6.13	6.30	6.31	5.96
y_{11}	1.09	1.08	4.98	5.32	2.36
y_{12}	1.04×10^6	1.04×10^6	1.04×10^6	1.04×10^6	1.04×10^6
y_{13}	11.06	11.06	11.06	11.06	11.06
y_{19}	1.23×10^{-3}	1.29×10^{-3}	1.53×10^{-3}	1.51×10^{-3}	1.36×10^{-3}
u_1	4.18×10^{-2}	4.12×10^{-2}	0	0	9.05×10^{-3}
u_2	0.45	0	0	0	0
u_3	3.19×10^{-3}	2.67×10^{-3}	1.05×10^{-3}	1.08×10^{-3}	1.95×10^{-3}
u_4	1.98	1.99	2.53	2.53	2.21
u_5	4.99×10^{-5}	5.15×10^{-5}	1.87×10^{-5}	0	0
u_6	6.30×10^4	6.30×10^4	6.30×10^4	6.30×10^4	6.30×10^4
u_{11}	5.92×10^{-3}	6.53×10^{-3}	1.03×10^{-2}	1.01×10^{-2}	7.77×10^{-3}

Table 14 – IAE and E_u values corresponding to: (a) NC_4 affected by each fault F_i, (b) reconfigurable controllers corresponding to F_1 and F_2.

	NC_4 (F_1)	RC_1	NC_4 (F_2)	RC_2	NC_4 (F_3)	NC_4 (F_4)
y_1	4099.9	4352.0	3795.6	2070.9	7988.7	3785.6
y_3	5078.7	4903.2	13,9056.6	64,963.2	5431.9	6096.4
y_7	14,141.9	14,572.8	11,272.9	10,247.9	11,103.5	11,273.6
y_8	17,553.2	36,663.3	10,452.9	6911.2	10,836.5	10,453.2
y_9	1728.6	911.8	1306.5	1394.2	1310.1	1306.5
y_{10}	6.30	6.26	6.21	48.15	50.26	5.96
y_{11}	2.87	1.51	2.36	1.43	2.39	2.36
y_{12}	1.04×10^6	1.04×10^6	1.04×10^6	1.04×10^6	1.04×10^6	1.01×10^6
y_{13}	11.06	11.06	11.06	11.06	11.06	833.61
y_{19}	1.45×10^{-3}	1.49×10^{-3}	1.36×10^{-3}	1.27×10^{-3}	1.42×10^{-3}	1.36×10^{-3}
u_1	1.21×10^{-2}	1.21×10^{-2}	9.05×10^{-3}	3.54×10^{-2}	8.74×10^{-3}	9.05×10^{-3}
u_2	0	0	0	2.72	0	0
u_3	1.75×10^{-3}	1.66×10^{-3}	8.47×10^{-4}	8.47×10^{-4}	8.42×10^{-4}	1.95×10^{-3}
u_4	2.30	2.28	2.50	0.55	0.19	2.21
u_5	0	1.24×10^{-4}	0	4.04×10^{-5}	0	0
u_6	6.30×10^4	6.30×10^4	6.30×10^4	6.30×10^4	6.30×10^4	2.71×10^4
u_{11}	8.41×10^{-3}	8.88×10^{-3}	7.77×10^{-3}	6.28×10^{-3}	8.65×10^{-3}	7.77×10^{-3}

Table 15 – IAE and E_u values corresponding to: (a) NC_4 affected by each fault F_i, (b) reconfigurable controllers corresponding to F_5 and F_6.

	NC_4 (F_5)	RC_5	NC_4 (F_6)	RC_6	NC_4 (F_7)	NC_4 (F_8)
y_1	4004.5	3589.7	3794.9	2048.4	8678.9	3785.6
y_3	4599.1	6159.1	90,508.3	50,233.1	5524.2	6096.4
y_7	16,246.4	10,192.9	11,272.9	10,248.5	11,044.9	11,273.6
y_8	13,239.2	6074.3	10,455.5	6911.3	10,862.5	10,453.2
y_9	1730.2	1426.2	1306.5	1394.3	1311.3	1306.5
y_{10}	6.29	6.17	6.21	46.93	57.20	5.96
y_{11}	4.92	1.34	2.36	1.43	2.40	2.36
y_{12}	1.04×10^6	1.04×10^6	1.04×10^6	1.04×10^6	1.04×10^6	1.03×10^6
y_{13}	11.06	11.06	11.06	11.06	11.06	528.82
y_{19}	1.50×10^{-3}	1.30×10^{-3}	1.36×10^{-3}	1.26×10^{-3}	1.43×10^{-3}	1.36×10^{-3}
u_1	7.65×10^{-4}	3.77×10^{-2}	9.05×10^{-3}	3.54×10^{-2}	8.67×10^{-3}	9.05×10^{-3}

(continued on next page)

Table 15 – (*continued*)

	NC_4 (F_5)	RC_5	NC_4 (F_6)	RC_6	NC_4 (F_7)	NC_4 (F_8)
u_2	0	0	0	2.65	0	0
u_3	1.18×10^{-3}	2.55×10^{-3}	3.99×10^{-4}	3.99×10^{-4}	1.33×10^{-3}	1.95×10^{-3}
u_4	2.50	2.03	2.42	0.55	0.01	2.21
u_5	0	4.77×10^{-5}	0	4.04×10^{-5}	0	0
u_6	6.30×10^{4}	6.30×10^{4}	6.30×10^{4}	6.30×10^{4}	6.30×10^{4}	1.28×10^{4}
u_{11}	9.82×10^{-3}	6.74×10^{-3}	7.77×10^{-3}	6.28×10^{-3}	8.87×10^{-3}	7.77×10^{-3}

REFERENCES

[1] Isermann R. Fault-diagnosis applications. Model-based condition monitoring: actuators, drives, machinery, plants, sensors, and fault-tolerant systems. Springer; 2011.

[2] Venkatasubramanian V, Rengaswamy R, Kavuri S. A review of process fault detection and diagnosis: part iii: process history based methods. Comput Chem Eng 2003;27(3):327–46.

[3] Mhaskar P, Liu J, Christofides P. Fault-tolerant process control. Methods and applications. Springer; 2013.

[4] Zhang Y, Jiang J. Bibliographical review on reconfigurable fault-tolerant control systems. Annu Rev Control 2008;32(2):229–52.

[5] Blanke M, Kinnaert M, Lunze J, Staroswiecki M. Diagnosis and fault-tolerant control. 2nd ed. Springer; 2006.

[6] Patton R. Fault-tolerant control: the 1997 situation, 3rd IFAC symposium on fault detection, supervision and safety for technical processes; 1997. p. 1033–55.

[7] Aprea J. Hydrogen energy demonstration plant in patagonia: description and safety issues. Int J Hydrogen Energy 2009;34:4684–91.

[8] Jiang J, Zhang Y. Accepting performance degradation in fault-tolerant control system design. IEEE Trans Control Syst Technol 2006;14(2):284–92.

[9] Boskovic J, Mehra R. Multiple-model adaptive flight control scheme for accommodation of actuator failures. J Guid Control Dyn 2002;25(4):712–24.

[10] Liu L, Shen Y, Dowell E, Zhu C. A general h_∞ fault tolerant control and management for a linear system with actuator faults. Automatica 2012;48:1676–82.

[11] Yang G, Wang J, Soh Y. Reliable h_∞ controller design for linear systems. Automatica 2001;37:717–25.

[12] Chilin D, Liu J, Chen X, Christofides P. Fault detection and isolation and fault tolerant control of a catalytic alkylation of benzene process. Chem Eng Sci 2012;78:155–66.

[13] Kale M, Chipperfield A. Stabilized mpc formulations for robust reconfigurable flight control. Control Eng Pract 2005;13(6):771–88.

[14] Yu X, Jiang J. Hybrid fault-tolerant flight control system design against partial actuator failures. IEEE Trans Control Syst Technol 2012;20(4):871–86.

[15] Chen J, Patton R, Chen Z. Active fault-tolerant flight control systems design using the linear matrix inequality method. Trans Inst Meas Control 1999;21(2):77–84.

[16] Alwi H, Edwards C. Fault tolerant control using sliding modes with on-line control allocation. Automatica 2008;44:1859–66.

[17] Hess R, Wells S. Sliding mode control applied to reconfigurable flight control design. J Guid Control Dyn 2003;26(3):452–62.

[18] Hamayun M, Edwards C, Alwi H. A fault tolerant control allocation scheme with output integral sliding modes. Automatica 2013;49:1830–7.

[19] Mirzaee A, Salahshoor K. Fault diagnosis and accommodation of nonlinear systems based on multiple-model adaptive unscented Kalman filter and switched mpc and h-infinity loop-shaping controller. J Process Control 2012;22:626–34.

[20] Kanev S, Verhaegan M. Controller reconfiguration for non-linear systems. Control Eng Pract 2000;8(11):1223–35.

[21] Jiang J, Yu X. Fault-tolerant control systems: a comparative study between active and passive approaches. Annu Rev Control 2012;36:60–72.

[22] Luppi P, Zumoffen D, Basualdo M. Decentralized plantwide control strategy for large-scale processes. Case study: pulp mill benchmark problem. Comput Chem Eng 2013;52:272–85.

[23] Zumoffen D. Oversizing analysis in plant-wide control design for industrial processes. Comput Chem Eng. http://dx.doi.org/http://dx.doi.org/10.1016/j.compchemeng.2013.03.021.

[24] Zumoffen D, Basualdo M. Avoiding oversizing in plant-wide control designs for industrial processes. Comput Aided Chem Eng 2012;30:937–41.

[25] Garcia C, Morari M. Internal model control. 2. Design procedure for multivariable systems. Ind Eng Chem Prod Res Dev 1985;24:472–84.

[26] Molina G, Zumoffen D, Basualdo M. Plant-wide control strategy applied to the Tennessee eastman process at two operating points. Comput Chem Eng 2011;35:2081–97.

[27] Sharifzadeh M, Thornhill N. Optimal selection of control structure using a steady-state inversely controlled process model. Comput Chem Eng 2012;38:126–38.

[28] Guler M, Clements S, Wills L, Heck B, Vachtsevanos G. Transition management for reconfigurable hybrid control systems. IEEE Control Syst Mag 2003;23(1):36–49.

[29] Nieto Degliuomini L, Biset S, Luppi P, Basualdo M. A rigorous computational model for hydrogen production from bio-ethanol to feed a fuel cell stack. Int J Hydrogen Energy 2012;37:3108–29.

[30] DieselNet. Emission test cycles. http://www.dieselnet.com/standards/cycles/; 2005.

[31] Downs J, Skogestad S. An industrial and academic perspective on plantwide control. Annu Rev Control 2011;35:99–110.

[32] Nieto Degliuomini L, Zumoffen D, Basualdo M. Plant-wide control design for fuel processor system with pemfc. Int J Hydrogen Energy 2012;37:14801–11.

[33] Kariwala V, Cao Y. Branch and bound method for multiobjective pairing selection. Automatica 2010;46:932–6.

[34] Rivera D. Internal model control. PID controller design. Ind Eng Chem Process Des Dev 1986;25:252–65.

[35] Van Overschee P, De Moor B. N4sid: subspace algorithms for the identification of combined deterministic-stochastic systems. Automatica 1994;30:75–93.

[36] Nieto Degliuomini L, Zumoffen D, Basualdo M. Low cost monitoring system for safe production of hydrogen from bio-ethanol. Int J Hydrogen Energy 2013;38:13872–83.